Stacking disorder and thermal transport properties of α-$RuCl_3$

Heda Zhang,[1] Michael A. McGuire,[1] Andrew F. May,[1] Hsin-Yun Chao,[2] Qiang Zheng,[1,3] Miaofang Chi,[2] Brian C. Sales,[1] David G. Mandrus,[1,3] Stephen E. Nagler,[4] Hu Miao,[1] Feng Ye,[4,*] and Jiaqiang Yan[1,†]

[1]*Materials Science and Technology Division, Oak Ridge National Laboratory, Oak Ridge, Tennessee 37831, USA*
[2]*Center for Nanophase Materials Sciences, Oak Ridge National Laboratory, Oak Ridge, Tennessee 37831, USA*
[3]*Department of Materials Science and Engineering, University of Tennessee, Knoxville, Tennessee 37996, USA*
[4]*Neutron Scattering Division, Oak Ridge National Laboratory, Oak Ridge, Tennessee 37831, USA*

(Received 3 May 2023; accepted 8 December 2023; published 8 January 2024)

α-$RuCl_3$, a well-known candidate material for Kitaev quantum spin liquid, is prone to stacking disorder due to the weak van der Waals bonding between the honeycomb layers. After a decade of intensive experimental and theoretical studies, the detailed correlation between stacking degree of freedom, structure transition, magnetic, and thermal transport properties remains unresolved. In this work, we reveal the effects of a small amount of stacking disorder inherent even in high quality α-$RuCl_3$ crystals. This small amount of stacking disorder results in the variation of the magnetic ordering temperature, and it suppresses the structure transition and thermal conductivity. Crystals with a minimal amount of stacking disorder have a $T_N > 7.4$ K and exhibit a well-defined structure transition around 140 K upon cooling. For those with more stacking faults and a T_N below 7 K, the structure transition occurs well below 140 K upon cooling and is incomplete, manifested by the diffuse streaks and the coexistence of both high-temperature and low-temperature phases down to the lowest measurement temperature. Both types of crystals exhibit oscillatory field-dependent thermal conductivity and a plateaulike feature in thermal Hall resistivity in the field-induced quantum spin liquid state. However, α-$RuCl_3$ crystals with a minimal amount of stacking disorder have a higher thermal conductivity that pushes the thermal Hall conductivity to be closer to the half-integer quantized value. These findings demonstrate a strong correlation between layer stacking, structure transition, magnetic, and thermal transport properties, underscoring the importance of interlayer coupling in α-$RuCl_3$ despite the weak van der Waals bonding.

DOI: 10.1103/PhysRevMaterials.8.014402

Shortly after the first experimental investigation of α-$RuCl_3$ as the candidate material for Kitaev quantum spin liquid [1], it was realized that the stacking sequence of the $RuCl_3$ honeycomb layers can affect the magnetic properties [2]. This is typical for van der Waals bonded cleavable magnets where nowadays the stacking degree of freedom of the two-dimensional structure units has been employed to engineer magnetic ground states [3–5]. The stacking of $RuCl_3$ honeycomb layers relative to each other leads to different proposed crystal structures, including the monoclinic $C2/m$, the rhombohedral $R\bar{3}$, and the trigonal $P3_112$. At room temperature, most studies reported a $C2/m$ structure for α-$RuCl_3$. Upon cooling, this monoclinic structure becomes unstable and around 150 K α-$RuCl_3$ goes through a first-order structure transition most likely to the rhombohedral $R\bar{3}$ structure [6]. In early studies of α-$RuCl_3$, more than one magnetic anomaly is typically observed in the temperature range 7–14 K [2,7–10]. The 14 K magnetic order seems to result from the $C2/m$ type stacking [8,11], and it is believed that the mixing of different types of stacking gives rise to the multiple magnetic anomalies in the temperature range 7–14 K.

With the intense materials synthesis effort, most α-$RuCl_3$ crystals being studied nowadays have only one single magnetic transition around $T_N = 7$ K. This has been employed as a simple and convenient criteria for a quick check of crystal quality. However, T_N has been found to vary from 6 to 8 K [12–14]. The origin of this discrepancy is still unknown. Also unknown is whether and how this magnetic order is correlated with the first-order structure transition at high temperatures.

Recently, the intensively debated thermal transport properties of α-$RuCl_3$ have called for a thorough revisiting of the materials issues of this fascinating compound [15]. The half-integer quantized thermal Hall conductance was believed to be one of the fingerprints for Majorana fermions of fractionalized spin excitations in α-$RuCl_3$. However, the thermal Hall conductance in field-induced disordered or the quantum spin liquid state was found to be sample-dependent, and the experimental observation of the half-integer quantized value requires using α-$RuCl_3$ crystals with high longitudinal thermal conductivity [16–22]. The other intriguing experimental observation is the oscillatory features of thermal conductivity as a function of in-plane magnetic field. These features were reproduced by different groups but the origin is under hot debate. While some believed this is an intrinsic character of the magnetic phase of $T_N \approx 7$ K [23,24] and attributed the observed oscillations to quantum oscillations of putative charge-neutral fermions [24], others believed that the

*yef1@ornl.gov
†yanj@ornl.gov

oscillatory features have an extrinsic origin and result from a sequence of field-induced magnetic phase transitions in crystals with stacking disorder [25,26].

All these interesting but debated results and interpretations highlight the importance of understanding the material issues in α-$RuCl_3$. In this work, we performed a careful investigation of the correlation between the layer stacking, structure transition, magnetic and thermal transport properties of different α-$RuCl_3$ crystals with T_N varying from 6 to 7.6 K. The amount of stacking disorder discussed in this work is far less than that in our previous work [23] and may not induce significant magnetic anomalies at 10–14 K in magnetic and specific-heat measurements. This small amount of stacking disorder causes the variations in T_N in different α-$RuCl_3$ crystals. Based on the characterizations, we categorize our α-$RuCl_3$ crystals into two types. Type-I α-$RuCl_3$ single crystals with T_N above 7.2 K have a minimal amount of stacking disorder and show a well-defined structure transition around 140 K upon cooling. For type-II crystals with more stacking disorder and a lower T_N around 6.5 K, the structure transition occurs below 140 K upon cooling and is incomplete, manifested by the coexistence of both high-temperature and low-temperature phases and the observation of diffuse streaks by neutron scattering below the structure transition. For both types of crystals, oscillatory field-dependent thermal conductivity and a plateaulike feature in thermal Hall resistivity were observed in the field-induced quantum spin liquid state. However, α-$RuCl_3$ single crystals with T_N above 7.4 K have a higher thermal conductivity, which pushes the thermal Hall conductivity to be closer to the half-integer quantized value. Our results demonstrate a strong correlation between the layer stacking, structure transition, magnetic, and thermal transport properties, and they highlight the importance of interlayer coupling in α-$RuCl_3$.

I. EXPERIMENTAL DETAILS

α-$RuCl_3$ used in this study was grown using two vapor transport techniques: self-selecting vapor growth with a small temperature gradient near the powder, and the conventional vapor transport technique with a large temperature gradient. The former is employed to grow thicker crystals for neutron single-crystal diffraction measurements described later, and the growth details can be found elsewhere [27]. The latter was performed in a two-zone tube furnace with the hot end kept at 1000 °C and the cold end at 750 °C. This yields millimeter-sized single crystals with a minimal amount of stacking disorder that are ideal for measurements of magnetic, thermodynamic, and thermal transport properties. The growth details were reported previously [23]. Varying the growth temperature and temperature gradient along the growth ampoule impacts the layer stacking and thus physical properties. For example, α-$RuCl_3$ crystals with T_N around 6 K were obtained by keeping the hot end of the growth ampoule at 1075 °C while the cold end was at 1025 °C. We noticed that crystal quality and properties are sensitive to the total vapor pressure inside of the growth ampoule. Our growths suggest that a higher vapor pressure facilitates the formation of stacking disorder, although a detailed relation has not been developed yet. Therefore, in order to obtain α-$RuCl_3$ crystals with a controlled degree of stacking disorder, all factors affecting the total vapor pressure inside of the growth ampoule should be considered, such as the purity and amount of starting powder, the volume of the growth ampoule, the growth temperature, and the temperature gradient along the growth ampoule. In our growths, high pure $RuCl_3$ powder synthesized by reacting RuO_2 powder with $AlCl_3$-KCl salt [28] or purchased from Furuya Metals (Japan) was used, and the growths were found to be comparable with respect to disorder control.

Elemental analysis on cleaved surfaces was performed using the wavelength dispersive (WDS) spectroscopy techniques. WDS measurement was performed using a JEOL JXA-8200X electron microprobe analyzer instrument equipped with five crystal-focusing spectrometers for wavelength dispersive x-ray spectroscopy. Magnetic properties were measured with a Quantum Design (QD) Magnetic Property Measurement System in the temperature range $2.0 \leqslant T \leqslant 300$ K. Specific-heat data below 30 K were collected using a QD Physical Property Measurement System (PPMS). Thermal transport measurements were performed on a custom-built PPMS puck as described before [23]. The temperature dependence of 0 0 l reflections was monitored on a flat surface by a PANalytical X'Pert Pro MPD powder x-ray diffractometer using Cu $K\alpha 1$ radiation. An Oxford PheniX closed-cycle cryostat was used to measure from 300 to 20 K.

Neutron diffraction experiments were carried out using the single-crystal diffractometer CORELLI [29] at SNS to monitor the structural phase transition and to search for potential diffuse scattering arising from possible stacking disorder in crystals grown under different conditions. Single crystals are mounted inside a closed-cycle refrigerator with a base temperature of 6 K. The MANTIDWORKBENCH package [30] was used for data reduction and analysis. We define the momentum transfer Q in three-dimensional (3D) reciprocal space in $Å^{-1}$ as $Q = Ha^* + Kb^* + Lc^*$, in which H, K, and L are Miller indices, and a^*, b^*, c^* are the lattice vectors in reciprocal space. For each type of crystal mentioned below, we checked one small piece around 6 mg and one large piece around 200 mg. No difference was observed between the small and large pieces.

II. RESULTS

Figure 1 shows the temperature dependence of magnetization, specific heat, and intensity of the 005 structural Bragg reflection (in $C2/m$ notation) illustrating the magnetic ordering and structure transition temperatures for two typical types of single crystals. We define the magnetic ordering temperature as the temperature where $Cp(T)$ peaks. Type-I crystals have $T_N > 7.2$ K and show sharp anomalies at T_N in both temperature dependence of magnetization and specific heat. The results of one crystal with $T_N = 7.6$ K [see Fig. 1(a)] are presented in this work as a representative of type-I crystals. For this crystal, abrupt changes in the temperature dependence of magnetization [Fig. 1(d)] and 005 reflection suggest the structure transition occurs at about 140 K upon cooling [Fig. 1(c)] and about 170 K upon warming [Fig. 1(e)]. Upon cooling below 140 K, the intensity of the peak sitting at $2\theta = 85.15°$ decreases quickly upon further cooling and disappears around 130 K. Meanwhile, a peak sitting at $2\theta = 85.62°$ appears and its intensity increases quickly upon cooling and

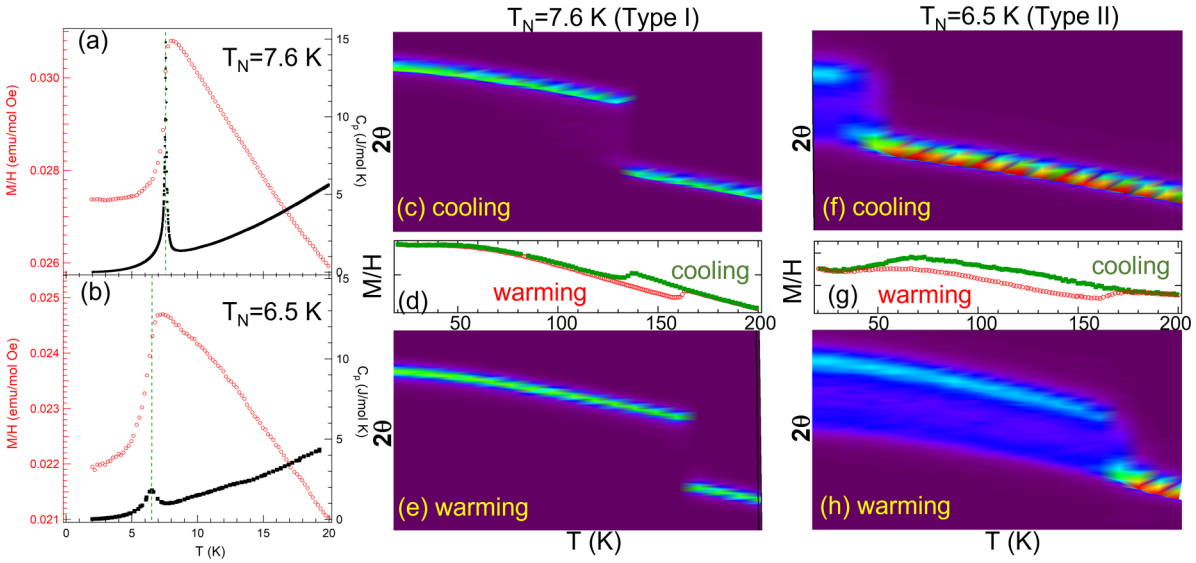

FIG. 1. Magnetic order and structure transition in two typical types of α-$RuCl_3$ single crystals. As described in the text, type-I crystals have magnetic ordering temperatures above 7.2 K, while type-II crystals normally order magnetically below 7 K. (a), (b) Temperature dependence of magnetization and specific heat (Cp) below 20 K. The magnetization was measured in a magnetic field of 1 kOe applied along the zigzag direction (perpendicular to the Ru-Ru bond). The vertical dashed lines highlight the Néel temperature, T_N, defined as the temperature where Cp peaks. $T_N = 7.6$ K in (a) is 1.1 K higher than that in (b). (c)–(e) Temperature dependence of magnetization and 005 reflection in the temperature range 20–200 K for the crystal with $T_N = 7.6$ K, a representative for type-I crystals. (f)–(h) Temperature dependence of magnetization and 005 reflection in the temperature range 20–200 K for the crystal with $T_N = 6.5$ K, an example for type-II crystals. The temperature dependence of magnetization in (d),(g) was measured in a magnetic field of 10 kOe applied perpendicular to the honeycomb plane. All data in [(c)–(h)] were collected in a temperature sweep at a rate of 2 K/min.

saturates below about 120 K. Steplike features associated with the structure transition are observed in the high-temperature magnetization at 140 and 170 K upon cooling and warming, respectively. Similar features are observed for all α-$RuCl_3$ crystals with T_N above 7.2 K.

Type-II crystals [Fig. 1(b)] normally have a T_N below 7 K and show broader transitions and weaker anomalies near T_N in magnetization and specific heat. Physical properties of one crystal with $T_N = 6.5$ K were presented in this work as an example of type-II crystals. Above T_N, some weak features were observed in both magnetization and specific heat in Fig. 1(b), in sharp contrast to Fig. 1(a). The structure transition also shows anomalous features distinct from those for type-I crystals. Upon cooling, the structure transition of the crystal with $T_N = 6.5$ K [see Fig. 1(f)] occurs around 60 K and the transition is not complete, which is well illustrated by the coexistence of reflections from both high-temperature and low-temperature phases to the lowest temperature 20 K of our x-ray diffraction measurement. Upon warming from 20 K, the phase coexistence persists until about 170 K, above which only the high-temperature monoclinic phase remains [Fig. 1(h)]. Accordingly, a wide loop was observed in the temperature dependence of magnetization [Fig. 1(g)]. It is interesting to note that for both α-$RuCl_3$ crystals the structure transition occurs around 170 K upon warming. When screening crystals, we noticed that the structure transition can occur in a wide temperature range 50–140 K when measuring upon cooling. For type-II crystals, the phase coexistence is always observed for crystals with T_N below 7 K. Figure S1 of the Supplemental Material [31] shows the x-ray diffraction results of two different crystals. Both crystals have $T_N = 7.1$ K (from specific heat) and the structure transition at 120 K upon cooling. However, one crystal shows a complete structure transition while the other one shows phase coexistence below 120 K, which seems to be the lowest structure transition temperature that one α-$RuCl_3$ crystal can have before showing a sluggish first-order structure transition and phase coexistence at low temperatures.

Considering the limited penetration depth of x-ray diffraction, we studied the structure of different pieces of pristine α-$RuCl_3$ crystals using single-crystal neutron diffraction. All crystals studied with neutron diffraction were well characterized by measuring magnetic properties and/or specific heat before exposing them to a neutron beam. Multiple pieces with mass ranging from 6 to 200 mg and T_N ranging from 6 to 7.6 K were checked. All crystals crystallize in $C2/m$ at room temperature but have a different degree of mosaic. We are aware of previous reports of successful growth of α-$RuCl_3$ crystals with the $P3_112$ structure [25]. Our neutron results do not rule out the possibility that some small crystals suitable for x-ray single-crystal diffraction can have $P3_112$ type structure. Figures 2(a) and 2(b) show the temperature dependence of (116) or (113) reflection to determine the structure transition in both crystals. For the crystal with $T_N = 7.6$ K, the structure transition occurs around 140 K upon cooling and 170 K upon warming, consistent with those determined from magnetic and x-ray diffraction measurements shown in Fig. 1. For the crystal with $T_N = 6.5$ K, the structure transition occurs below 80 K upon cooling and 170 K upon warming. The latter temperature agrees well with those determined from magnetic and x-ray diffraction measurements shown in Fig. 1. The slightly different transition temperature when measuring

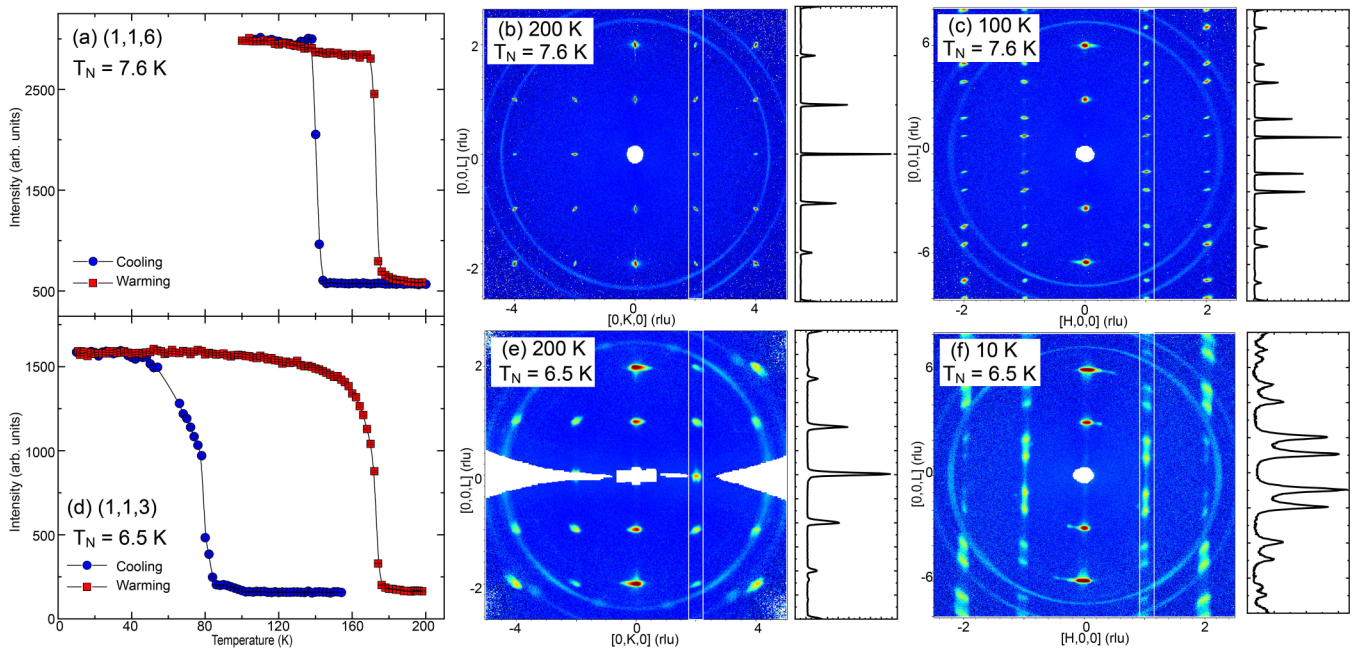

FIG. 2. Neutron single-crystal diffraction found a sharp structure transition for the crystal with $T_N = 7.6$ K but a sluggish structure transition and diffuse streaks for the crystal with $T_N = 6.5$ K. (a) The thermal evolution of the (1,1,6) reflection measured in cooling and warming at a rate of 2K/min confirms the sharp structural transition in the crystal with $T_N = 7.6$ K. (b), (c) The neutron diffraction patterns at 200 K (in the high-temperature $C/2m$ phase) and 100 K (in the low-temperature $R\bar{3}$ phase) for the crystal with $T_N = 7.6$ K. Extra reflections in (c) confirm the symmetry change at low temperatures. (d) The temperature evolution of (1,1,3) reflection measured in cooling and warming at a rate of 2 K/min of the crystal with $T_N = 6.5$ K. (e), (f) The neutron diffraction patterns at 200 K (in the high-temperature $C/2m$ phase) and 10 K (in the low-temperature $R\bar{3}$ phase) for the crystal with $T_N = 6.5$ K. The mosaic in (e) and the diffuse streaks in (f) are highlighted by the line cut shown in the right half of each panel (b), (c), (e), and (f). The transformation matrixes between the high-T $C2/m$ and low-T $R\bar{3}$ unit cell are $\mathbf{a}_r = \mathbf{a}_m$, $\mathbf{b}_r = 1/2(-\mathbf{a}_m + \mathbf{b}_m)$, $\mathbf{c}_r = \mathbf{a}_m + 3\mathbf{c}_m$, where the subscripts "$r$" and "$m$" denote the rhombohedral and monoclinic structures.

cooling is in line with the fact that this transition temperature can vary in a wide temperature range 50–140 K depending on the concentration and detailed distribution of stacking imperfection.

Detailed reciprocal space maps provide a better understanding of the nature of average and local structure for both α-$RuCl_3$ single crystals. Figures 2(b) and 2(c) show the neutron diffraction patterns collected at 200 K (above the structure transition) and 100 K (below the structure transition) for the type-I crystal with $T_N = 7.6$ K. As reported previously, the high-temperature monoclinic $C2/m$ structure becomes unstable upon cooling and transforms into a rhombohedral $R\bar{3}$ structure [6]. This can be appreciated by the appearance of additional Bragg peaks along the L direction [see Fig. 2(c)]. The right half of each panel shows the line cut along $[0, 2, L]$ highlighting (i) that this crystal is of high quality with negligible mosaic, and (ii) the absence of any diffuse feature in the temperature range investigated. The correlation length ξ derived from the full width at half-maximum (FWHM) of the (0,2,0) reflection at 200 K using a Lorentzian line shape is $\sim 450 \pm 10$ Å, which is at the resolution limit of the neutron measurement. The peak broadens slightly at 100 K and suggests a reduction of the correlation length to about 350 ± 10 Å. Figures 2(e) and 2(f) show the neutron diffraction patterns at 200 K (above the structure transition) and 10 K (below the structure transition) for the type-II crystal with $T_N = 6.5$ K. The crystal clearly has a much larger mosaic, and more interestingly, diffuse streaks are evident below the structural transition [Fig. 2(f)]. The correlation length is about 78 ± 5 Å at 200 K and reduces to 32 ± 3 Å at 10 K. Both values are much smaller compared to those for the crystal with $T_N = 7.6$ K. Despite the apparent difference in the correlation lengths, the local environment surrounding the Ru ions for both single crystals is very similar in the high-temperature $C2/m$ phase. As can be determined from the structure information listed in Table I in the Supplemental Material [31], those two crystals have the same lattice parameters, Cl-Ru-Cl bond angles, and Ru-Cl bond lengths at 200 K. Given the surprisingly similar crystal structure and lack of any unidentified phase, the observed diffuse streaks in the crystal with $T_N = 6.5$ K are attributed to the stacking faults that are prevalent in van der Waals bonded layered materials. As discussed later, the stacking disorder can act as the pinning center preventing a uniform structure phase transition. Thus the structure transition occurs at a lower temperature. The inhomogeneous distribution of stacking disorder might be responsible for the sluggish transition occurring in a wider temperature range.

After warming above the structure transition, both crystals seem to get back to the original pristine state. In the Supplemental Material [31], we show the neutron diffraction patterns of both crystals after warming up to 200 K from below the structure transition. Interestingly, the diffraction pattern and the correlation length are comparable before and after the thermal cycling. We also monitored the possible effects of thermal cycling on the structure transition and magnetic order by

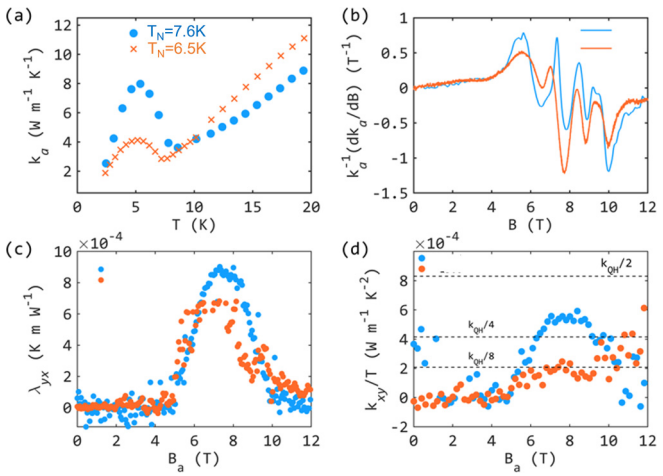

FIG. 3. Thermal transport measurement results of α-$RuCl_3$. (a) Thermal conductivity of α-$RuCl_3$ crystal. Heat current is applied along the zigzag direction (perpendicular to the Ru-Ru bond). (b) Oscillatory features of thermal conductivity. Data collected with both heat current and magnetic field along the zigzag direction. (c),(d) Thermal Hall resistivity (c) and conductivity (d) at 5 K. Both heat current and magnetic field are applied along the zigzag direction. The horizontal dashed lines in (d) highlight the thermal Hall conductivity relative to the fraction of quantized thermal Hall κ_{QH}/n, where $n = 2$, 4, and 8 are shown.

measuring the temperature dependence of magnetization and specific heat. As shown in the Supplemental Material [31], the thermal cycling does not seem to affect the magnetic order after 10 thermal cycles.

Figure 3(a) shows the typical temperature dependence of thermal conductivity (κ_a, thermal current along a-axis) of both single crystals below 20 K. The small difference in T_N can be well resolved. Both samples show a recovery of heat transport upon cooling through T_N and a peak around 5 K in the temperature dependence of thermal conductivity. This is consistent with previous reports [19,22,32–34]. The crystal with $T_N = 7.6$ K has a higher thermal conductivity below T_N. This magnitude of thermal conductivity is higher than the threshold value for the observation of the half-integer quantized thermal Hall effect [22].

Figure 3(b) shows the oscillatory features in the field dependence of longitudinal thermal conductivity (κ_a) at 2 K, shown as the scaled derivative ($\kappa^{-1}d\kappa/dB$ T^{-1}) of thermal conductivity with respect to applied magnetic field. This scaling procedure brings the oscillatory features of various samples with different thermal conductivities to the same scale and emphasizes the critical fields instead of absolute oscillatory amplitudes. We observed that the oscillatory features, especially those after the system has entered the field-induced quantum spin liquid phase (7.5 T), are very similar for both samples. This indicates that the oscillatory features in the field-induced quantum spin liquid region are dominated by in-plane physics.

We also studied the thermal Hall effect of both crystals. Figures 3(c) and 3(d) show a plateau region in both thermal resistivity and (scaled) conductivity measured at 5 K. The plateau spans the field region in which the field-induced disordered or quantum spin liquid phase dominates. The profile of the thermal Hall signal is better shown by resistivity. The scaled thermal Hall conductivity is highly sample-dependent. We noticed in our sample screening that the plateau value could vary by a factor of 5 for different samples with different thermal conductivities. The crystal with $T_N = 7.6$ K has less stacking disorder and hence a higher thermal conductivity. This leads to a near half-integer quantized κ_{xy}/T. In contrast, κ_{xy}/T for the crystal with $T_N = 6.5$ K is further away from the half-integer quantized value as illustrated by the data shown in Fig. 3(d). As reported in Ref. [23], the evolution of thermal Hall resistivity with temperature in all samples measured in this work shows one feature associated with the suppression of T_N and the other one at the crossover from the field-induced quantum spin liquid state and the partially polarized state. A plateau is normally observed when these two features are of comparable magnitude, signaling caution is needed when explaining the significance of the plateau in thermal Hall conductivity.

III. DISCUSSIONS

The detailed physical properties of two α-$RuCl_3$ crystals were reported in this work as the representatives of two types of α-$RuCl_3$ crystals. Typically, type-I crystals have a T_N above 7.2 K, whereas type-II crystals have a T_N below 7 K. Specific-heat results shown in Fig. 1 and Fig. S5 in the Supplemental Material [31] demonstrate that T_N of our α-$RuCl_3$ crystals can range from 6 to 7.6 K. Our WDS measurements confirmed that all crystals have the same atomic ratio and the *nonstoichiometry or chemical composition should not be responsible for the variation in T_N among different α-$RuCl_3$ crystals*. Therefore, the differences in properties between type-I and type-II crystals may shed some light on the origin of T_N variation in different α-$RuCl_3$ crystals.

A careful comparison between type-I and -II crystals indicates that *stacking disorder causes a sluggish structure transition and leads to phase coexistence at low temperatures*. Type-II crystals distinguish themselves from type-I crystals by showing a sluggish structure transition most likely originating from the stacking disorder. The larger mosaic [see Fig. 2(e)] suggests the presence of stacking disorder in type-II crystals. From magnetic and x-ray and neutron diffraction measurements of different crystals, the structure transition when being measured upon cooling occurs at a lower temperature with increasing stacking disorder, and two-phase coexistence is always observed when the structure transition occurs below 120 K. The phase coexistence was observed at 20 K, the lowest temperature of our x-ray diffraction measurements. It will not be a surprise if the phase coexistence persists at even lower temperatures, for example below T_N. Our x-ray and neutron diffraction studies provide solid evidence for the phase coexistence but cannot tell the detailed concentration and distribution of those two phases or the stacking disorder. However, one can expect that the stacking disorder acts as a pinning center for the sliding of $RuCl_3$ honeycomb layers during the structure phase transition, leading to more complex stacking disorder as the temperature decreases. This expectation is consist with the observation of diffuse streaks for type-II crystals shown in Fig. 2(f). Such diffuse streaks were observed in previous studies and attributed to stack-

ing disorder between $RuCl_3$ honeycomb layers [8,12]. The concentration and detailed distribution of stacking disorder in the starting crystals affect the mosaic, structure transition temperature, the concentration, and distribution of both high-temperature and low-temperature phases below the structure transition. Figure S1 presents the x-ray diffraction results for crystals with T_N near 7.1 K, which highlights the effect of the concentration and detailed distribution of stacking disorder.

The neutron single-crystal diffraction confirms that type-I crystals are of high quality as evidenced by a large correlation length beyond the resolution limit of our neutron measurement. However, this does not mean that these crystals are free of stacking disorder. Previously, a scanning transmission electron microscope (STEM) study observed $P3_112$-type stacking in α-$RuCl_3$ flakes from one crystal with $C2/m$ structure determined by neutron single-crystal diffraction [35]. This result was reproduced in our recent STEM studies. STEM probes a small region of a thin flake, while neutron diffraction studies the whole crystal in neutron beam averaging over many similar and different regions. The discrepancy between STEM and neutron diffraction indicates the presence of stacking disorder in type-I crystals, and the disorder can even exist in local regions in the form of other types of layer stacking with comparable energy [11]. Nevertheless, the long coherence length implies that the concentration of stacking disorder in high-quality type-I crystals is low.

The stacking disorder can be responsible for the slightly suppressed T_N. The phase coexistence or stacking disorder may affect both the interlayer and intralayer magnetic interactions. The interlayer magnetic interactions are disrupted by inhomogeneous layer spacing and exchange paths, while theoretical studies have shown that the intralayer exchange interactions are influenced by the stacking structure [36]. Neutron single-crystal diffraction at 200 K revealed the same local structure in both types of α-$RuCl_3$ crystals. However, whether the local structure similarity persists at low temperatures is unknown. Despite tremendous efforts, the low-temperature structure is not yet determined due to the appearance of diffuse scattering below the structure transition [8,11]. Solving the low-temperature structure is beyond the scope of current effort. However, we would point out that this is essential to resolve possible local distortion of $RuCl_6$ octahedra that determines the relative magnitude of those terms in magnetic Hamiltonian and also critical for a quantitative understanding of the suppression of T_N. In addition, the phase coexistence scenario should be considered when solving the low-temperature structure, depending on the quality of crystals employed.

The above discussion of how stacking disorder suppresses T_N does not contradict the previous proposal that mechanical deformation can induce magnetic anomalies in the temperature range 10–14 K [11,23]. In previous studies, mechanical deformation was employed to create a large concentration of stacking disorder, which resulted in crystals with one single magnetic order at 14 K. However, the concentration of stacking disorder in both types of crystals studied in this work is much lower, and this is especially true for type-I crystals. On the other hand, the suppression of T_N from 7 K and the appearance of weak magnetic anomalies in the temperature range 10–14 K seem to be strongly correlated and may have the same origin. The Supplemental Material [31] presents specific-heat data for more samples, with separate panels highlighting the features below and above 8 K. For those crystals with suppressed T_N (for example lower than 7 K) or with more than one lambda-type anomaly, some weak anomalies can be observed above 8 K. All the observations suggest that a small amount of stacking disorder suppresses the long-range magnetic order with T_N around 7 K, and increasing the population of stacking faults leads to magnetic phases with T_N above 10 K.

The stacking disorder is also responsible for the sample-dependent thermal transport properties. Upon cooling through T_N, type-I crystals show a stronger recovery of thermal conductivity [see Fig. 3(a)]. The high thermal conductivity and T_N of type-I crystals indicate the importance of interlayer coupling and interactions. As reported previously [18,22], a large thermal conductivity is necessary for the observation of half-integer quantized thermal Hall effect. In Fig. 3(d), the crystal with $T_N = 7.6$ K shows a high thermal Hall conductivity κ_{xy}/T, closer to the half-integer quantized value. It is interesting to note that the half-integer quantized thermal Hall effect was recently observed for a deformed α-$RuCl_3$ crystal with $T_N = 14$ K, which exhibits a high thermal Hall resistivity despite a low thermal conductivity [23]. These two studies suggest two different ways to observe thermal Hall conductivity at half-integer quantized value: using high-quality samples with a minimal amount of stacking disorder and high thermal conductivity, or using samples with a high thermal Hall resistivity. Obviously, thermal Hall conductivity can be rather sample-dependent, and the stacking disorder can have a dramatic effect on it. Despite the sample-dependent thermal Hall conductivity, both types of crystals have similar critical fields for oscillatory features in magnetothermal conductivity and also the same field range in which the thermal Hall effect and oscillatory features in thermal conductivity are observed.

The correlation between stacking disorder, magnetic, and thermal transport properties developed in this work suggests the following can be *valid criteria when selecting crystals with a minimal amount of stacking disorder*: (i) the structure transition temperature measured upon cooling. This can be determined by measuring the temperature dependence of magnetization in the paramagnetic state, or by monitoring the evolution with temperature of an appropriate nuclear reflection by x-ray or neutron diffraction. (ii) The magnetic ordering temperature determined by specific-heat measurements. In addition to a well-defined T_N, specific-heat measurements can also tell whether extra anomalies exist near T_N (see Fig. S5). We noticed that the anisotropic magnetic susceptibility around T_N is not that sensitive to the small variation of T_N or the presence of multiple magnetic transitions as revealed by specific heat shown in Fig. S5. From the characterizations of different crystals in the past decade, crystals with a minimal amount of stacking disorder should have a structure transition around 140 K when being measured upon cooling and one single magnetic anomaly around 7.6 K in specific heat.

IV. SUMMARY

In summary, we study the effects of a small amount of stacking disorder on the structure, magnetic, and ther-

mal transport properties in α-$RuCl_3$ single crystals with T_N varying from 6.0 to 7.6 K. The amount of stacking disorder may not be enough to induce magnetic anomalies in the temperature range 10–14 K, but it can still have a dramatic effect on the physical properties. The stacking disorder in as-grown crystals can suppress the structure transition temperature (upon cooling), the Néel temperature, and lattice thermal conductivity. The similar oscillatory field-dependent thermal conductivity and plateaulike feature in thermal Hall resistivity were observed in all α-$RuCl_3$ single crystals studied in this work despite the variation in T_N. However, α-$RuCl_3$ single crystals with a minimal amount of stacking disorder have a higher thermal conductivity, which pushes the thermal Hall conductivity to be closer to the half-integer quantized value. Our results demonstrate a strong correlation between the layer stacking, structure transition, magnetic, and thermal transport properties, and they highlight the importance of interlayer coupling in α-$RuCl_3$ despite the weak van der Waals bonding. Our work also suggests well-defined criteria for selecting α-$RuCl_3$ crystals with a minimal amount of stacking disorder: a structure transition around 140 K when being measured upon cooling and one single magnetic anomaly around 7.6 K in specific heat. Moreover, the presence of stacking disorder may be universal in all layered, cleavable magnets. The implications of this work can be extended to other compounds and help resolve and understand their intrinsic properties and the novel quantum phenomena.

ACKNOWLEDGMENTS

J.Y. gratefully acknowledges discussions with Tom Berlijn, Huibo Cao, Hwan Do, and Alan Tennant. The authors thank Michael Lance for WDS measurements. H.Z., S.N., M.M., and J.Y. were supported by the U.S. Department of Energy, Office of Science, National Quantum Information Science Research Centers, Quantum Science Center. Q.Z., D.M., A.M., H.M., and B.S. were supported by the U.S. Department of Energy, Office of Science, Basic Energy Sciences, Materials Sciences and Engineering Division. J.C. and M.C. were supported by an Early Career project supported by DOE Office of Science FWP ERKCZ55. A portion of this research used resources at the Spallation Neutron Source, a DOE Office of Science User Facility operated by the Oak Ridge National Laboratory. This manuscript has been authored by UT-Battelle, LLC, under Contract No. DE-AC0500OR22725 with the U.S. Department of Energy. The United States Government retains and the publisher, by accepting the article for publication, acknowledges that the United States Government retains a nonexclusive, paid-up, irrevocable, worldwide license to publish or reproduce the published form of this manuscript, or allow others to do so, for the United States Government purposes. The Department of Energy will provide public access to these results of federally sponsored research in accordance with the DOE Public Access Plan [37].

[1] K. W. Plumb, J. P. Clancy, L. J. Sandilands, V. V. Shankar, Y. F. Hu, K. S. Burch, H.-Y. Kee, and Y.-J. Kim, α-$RuCl_3$: A spin-orbit assisted mott insulator on a honeycomb lattice, Phys. Rev. B **90**, 041112(R) (2014).

[2] A. Banerjee, C. A. Bridges, J.-Q. Yan, A. A. Aczel, L. Li, M. B. Stone, G. E. Granroth, M. D. Lumsden, Y. Yiu, J. Knolle *et al.*, Proximate kitaev quantum spin liquid behaviour in a honeycomb magnet, Nat. Mater. **15**, 733 (2016).

[3] B. Huang, G. Clark, E. Navarro-Moratalla, D. R. Klein, R. Cheng, K. L Seyler, D. Zhong, E. Schmidgall, M. A. McGuire, D. H. Cobden *et al.*, Layer-dependent ferromagnetism in a van der waals crystal down to the monolayer limit, Nature (London) **546**, 270 (2017).

[4] W. Chen, Z. Sun, Z. Wang, L. Gu, X. Xu, S. Wu, and C. Gao, Direct observation of van der waals stacking–dependent interlayer magnetism, Science **366**, 983 (2019).

[5] J.-Q. Yan, Perspective–the elusive quantum anomalous hall effect in $MnBi_2Te_4$: Materials, ECS J. Solid State Sci. Technol. **11**, 063007 (2022).

[6] S. Mu, K. D. Dixit, X. Wang, D. L. Abernathy, H. Cao, S. E. Nagler, J. Yan, P. Lampen-Kelley, D. Mandrus, C. A. Polanco, L. Liang, G. B. Halász, Y. Cheng, A. Banerjee, and T. Berlijn, Role of the third dimension in searching for majorana fermions in α-$RuCl_3$ via phonons, Phys. Rev. Res. **4**, 013067 (2022).

[7] Y. Kubota, H. Tanaka, T. Ono, Y. Narumi, and K. Kindo, Successive magnetic phase transitions in α-$RuCl_3$: Xy-like frustrated magnet on the honeycomb lattice, Phys. Rev. B **91**, 094422 (2015).

[8] R. D. Johnson, S. C. Williams, A. A. Haghighirad, J. Singleton, V. Zapf, P. Manuel, I. I. Mazin, Y. Li, H. O. Jeschke, R. Valentí, and R. Coldea, Monoclinic crystal structure of α-$RuCl_3$ and the zigzag antiferromagnetic ground state, Phys. Rev. B **92**, 235119 (2015).

[9] J. A. Sears, M. Songvilay, K. W. Plumb, J. P. Clancy, Y. Qiu, Y. Zhao, D. Parshall, and Y.-J. Kim, Magnetic order in α-$RuCl_3$: A honeycomb-lattice quantum magnet with strong spin-orbit coupling, Phys. Rev. B **91**, 144420 (2015).

[10] M. Majumder, M. Schmidt, H. Rosner, A. A. Tsirlin, H. Yasuoka, and M. Baenitz, Anisotropic $Ru^3 + 4d^5$ magnetism in the α-$RuCl_3$ honeycomb system: Susceptibility, specific heat, and zero-field nmr, Phys. Rev. B **91**, 180401(R) (2015).

[11] H. B. Cao, A. Banerjee, J.-Q. Yan, C. A. Bridges, M. D. Lumsden, D. G. Mandrus, D. A. Tennant, B. C. Chakoumakos, and S. E. Nagler, Low-temperature crystal and magnetic structure of α-$RuCl_3$, Phys. Rev. B **93**, 134423 (2016).

[12] S. Kim, B. Yuan, and Y.-J. Kim, α-$RuCl_3$ and other kitaev materials, APL Mater. **10**, 080903 (2022).

[13] J. A. Sears, Y. Zhao, Z. Xu, J. W. Lynn, and Y.-J. Kim, Phase diagram of α-$RuCl_3$ in an in-plane magnetic field, Phys. Rev. B **95**, 180411(R) (2017).

[14] S.-H. Do, S.-Y. Park, J. Yoshitake, J. Nasu, Y. Motome, Y. S. Kwon, D. T. Adroja, D. J. Voneshen, K. Kim, T.-H. Jang *et al.*,

Majorana fermions in the kitaev quantum spin system α-$RuCl_3$, Nat. Phys. **13**, 1079 (2017).

[15] P. Lee, Quantized (or not quantized) thermal hall effect and oscillations in the thermal conductivity in the kitaev spin liquid candidate $RuCl_3$, J. Club Condens. Matter Phys. doi:10.36471/JCCM_November_2021_02.

[16] T. Yokoi, S. Ma, Y. Kasahara, S. Kasahara, T. Shibauchi, N. Kurita, H. Tanaka, J. Nasu, Y. Motome, C. Hickey *et al.*, Half-integer quantized anomalous thermal hall effect in the kitaev material candidate α-$RuCl_3$, Science **373**, 568 (2021).

[17] Y. Kasahara, T. Ohnishi, Y. Mizukami, O. Tanaka, S. Ma, K. Sugii, N. Kurita, H. Tanaka, J. Nasu, Y. Motome *et al.*, Majorana quantization and half-integer thermal quantum hall effect in a kitaev spin liquid, Nature (London) **559**, 227 (2018).

[18] M. Yamashita, J. Gouchi, Y. Uwatoko, N. Kurita, and H. Tanaka, Sample dependence of half-integer quantized thermal hall effect in the kitaev spin-liquid candidate α-$RuCl_3$, Phys. Rev. B **102**, 220404(R) (2020).

[19] É. Lefrançois, G. Grissonnanche, J. Baglo, P. Lampen-Kelley, J.-Q. Yan, C. Balz, D. Mandrus, S. E. Nagler, S. Kim, Y.-J. Kim, N. Doiron-Leyraud, and L. Taillefer, Evidence of a phonon hall effect in the kitaev spin liquid candidate α-$RuCl_3$, Phys. Rev. X **12**, 021025 (2022).

[20] P. Czajka, T. Gao, M. Hirschberger, P. Lampen-Kelley, A. Banerjee, N. Quirk, D. G. Mandrus, S. E. Nagler, and N. P. Ong, Planar thermal hall effect of topological bosons in the kitaev magnet α-$RuCl_3$, Nat. Mater. **22**, 36 (2022).

[21] J. Bruin, R. R. Claus, Y. Matsumoto, N. Kurita, H. Tanaka, and H. Takagi, Robustness of the thermal hall effect close to half-quantization in α-$RuCl_3$, Nat. Phys. **18**, 401 (2022).

[22] Y. Kasahara, S. Suetsugu, T. Asaba, S. Kasahara, T. Shibauchi, N. Kurita, H. Tanaka, and Y. Matsuda, Quantized and unquantized thermal hall conductance of the kitaev spin liquid candidate α-$RuCl_3$, Phys. Rev. B **106**, L060410 (2022).

[23] H. Zhang, A. May, H. Miao, B. Sales, D. Mandrus, S. Nagler, M. McGuire, and J. Yan, The sample-dependent and sample-independent thermal transport properties of α-$RuCl_3$, Phys. Rev. Mater. **7**, 114403 (2023).

[24] P. Czajka, T. Gao, M. Hirschberger, P. Lampen-Kelley, A. Banerjee, J. Yan, D. G. Mandrus, S. E. Nagler, and N. P. Ong, Oscillations of the thermal conductivity in the spin-liquid state of α-$RuCl_3$, Nat. Phys. **17**, 915 (2021).

[25] J. Bruin, R. R. Claus, Y. Matsumoto, J. Nuss, S. Laha, B. V. Lotsch, N. Kurita, H. Tanaka, and H. Takagi, Origin of oscillatory structures in the magnetothermal conductivity of the putative kitaev magnet α-$RuCl_3$, APL Mater. **10**, 090703 (2022).

[26] É. Lefrançois, J. Baglo, Q. Barthélemy, S. Kim, Y.-J. Kim, and L. Taillefer, Oscillations in the magnetothermal conductivity of α-$RuCl_3$: Evidence of transition anomalies, Phys. Rev. B **107**, 064408 (2023).

[27] J.-Q. Yan and M. A. McGuire, Self-selecting vapor growth of transition metal halide single crystals, Phys. Rev. Mater. **7**, 013401 (2023).

[28] J.-Q. Yan, B. C. Sales, M. A. Susner, and M. A. Mcguire, Flux growth in a horizontal configuration: an analog to vapor transport growth, Phys. Rev. Mater. **1**, 023402 (2017).

[29] F. Ye, Y. Liu, R. Whitfield, R. Osborn, and S. Rosenkranz, Implementation of cross correlation for energy discrimination on the time-of-flight spectrometer CORELLI, J. Appl. Crystallogr. **51**, 315 (2018).

[30] O. Arnold *et al.*, MantidData analysis and visualization package for neutron scattering and uSR experiments, Nuclear Instruments and Methods in Physics Research Section A: Accelerators, Spectrometers, Detectors and Associated Equipment **764**, 156 (2014).

[31] See Supplemental Material at http://link.aps.org/supplemental/10.1103/PhysRevMaterials.8.014402. for (1) Temperature dependence of (005) reflection for two pieces of crystals with T_N about 7.1 K, (2) Neutron diffraction data at 200 K before and after thermal cycle, (3) Magnetization and specific heat in different thermal cycles, (4) Specific heat near 7 K of different crystals, (5) Structure details determined from neutron single crystal diffraction at 200 K.

[32] R. Hentrich, A. U. B. Wolter, X. Zotos, W. Brenig, D. Nowak, A. Isaeva, T. Doert, A. Banerjee, P. Lampen-Kelley, D. G. Mandrus, S. E. Nagler, J. Sears, Y. J. Kim, B. Buchner, and C. Hess, Unusual phonon heat transport in α-$RuCl_3$: strong spin-phonon scattering and field-induced spin gap, Phys. Rev. Lett. **120**, 117204 (2018).

[33] D. Hirobe, M. Sato, Y. Shiomi, H. Tanaka, and E. Saitoh, Magnetic thermal conductivity far above the néel temperature in the kitaev-magnet candidate α-$RuCl_3$, Phys. Rev. B **95**, 241112(R) (2017).

[34] I. A. Leahy, C. A. Pocs, P. E. Siegfried, D. Graf, S.-H. Do, K.-Y. Choi, B. Normand, and M. Lee, Anomalous thermal conductivity and magnetic torque response in the honeycomb magnet α-$RuCl_3$, Phys. Rev. Lett. **118**, 187203 (2017).

[35] M. Ziatdinov, A. Banerjee, A. Maksov, T. Berlijn, W. Zhou, H. B. Cao, J.-Q. Yan, C. A. Bridges, D. G. Mandrus, S. E. Nagler *et al.*, Atomic-scale observation of structural and electronic orders in the layered compound α-$RuCl_3$, Nat. Commun. **7**, 13774 (2016).

[36] H.-S. Kim and H.-Y. Kee, Crystal structure and magnetism in α-$RuCl_3$: An ab initio study, Phys. Rev. B **93**, 155143 (2016).

[37] http://energy.gov/downloads/doe-public-access-plan.